J|A|C|S ARTICLES

Published on Web 11/30/2010

Stabilization of Amorphous Calcium Carbonate in Inorganic Silica-Rich Environments

Matthias Kellermeier,[†] Emilio Melero-García,[‡] Fabian Glaab,[†] Regina Klein,[†] Markus Drechsler,[§] Reinhard Rachel,[||] Juan Manuel García-Ruiz,[‡] and Werner Kunz*,[†]

Institute of Physical and Theoretical Chemistry, University of Regensburg, Universitätsstrasse 31, D-93040 Regensburg, Germany, Laboratorio de Estudios Crystalográficos, IACT (CSIC-UGR), Avda. del Conocimiento s/n, P.T. Ciencias de la Salud, E-18100 Armilla, Spain, Institute of Macromolecular Chemistry, University of Bayreuth, Universitätsstrasse 30, D-95440 Bayreuth, Germany, and Institute of Microbiology and Archaeal Center, University of Regensburg, Universitätsstrasse 31, D-93040 Regensburg, Germany

Received August 4, 2010; E-mail: werner.kunz@chemie.uni-regensburg.de

Abstract: In biomineralization, living organisms carefully control the crystallization of calcium carbonate to create functional materials and thereby often take advantage of polymorphism by stabilizing a specific phase that is most suitable for a given demand. In particular, the lifetime of usually transient amorphous calcium carbonate (ACC) seems to be thoroughly regulated by the organic matrix, so as to use it either as an intermediate storage depot or directly as a structural element in a permanently stable state. In the present study, we show that the temporal stability of ACC can be influenced in a deliberate manner also in much simpler purely abiotic systems. To illustrate this, we have monitored the progress of calcium carbonate precipitation at high pH from solutions containing different amounts of sodium silicate. It was found that growing ACC particles provoke spontaneous polymerization of silica in their vicinity, which is proposed to result from a local decrease of pH nearby the surface. This leads to the deposition of hydrated amorphous silica layers on the ACC grains, which arrest growth and alter the size of the particles. Depending on the silica concentration, these skins have different thicknesses and exhibit distinct degrees of porosity, therefore impeding to varying extents the dissolution of ACC and energetically favored transformation to calcite. Under the given conditions, crystallization of calcium carbonate was slowed down over tunable periods or completely prevented on time scales of years, even when ACC coexisted side by side with calcite in solution.

1. Introduction

The hard parts of living organisms often feature intriguing morphologies, textures, and an elaborate hierarchical structure designed to fulfill a wide range of specific tasks, from protection to gravity perception and balance sensing. These materials usually consist of an inorganic mineral and an intimately associated organic matrix of biological macromolecules, which control the mineralization process leading to complex hybrid structures.[1] One of the most common minerals in biogenic sources is calcium carbonate, which mainly occurs in the form of the crystalline polymorphs calcite and aragonite. Prominent examples include mollusk nacre or the coccoliths produced by certain marine algae.

In recent years, an increasing amount of evidence has been collected suggesting that amorphous calcium carbonate (ACC) plays a far greater role in biomineralization than previously suspected.[2] ACC is the thermodynamically least stable among all $CaCO_3$ polymorphs. However, being amorphous, its formation is kinetically favored and thus it is frequently observed first in the course of precipitation from solution, to subsequently transform more or less rapidly toward phases of higher stability, eventually calcite under ambient conditions.[3−5] Living organisms can obviously thwart the spontaneous transformation of ACC in a deliberate manner, given that stable ACC has been identified as a major structural element in some biominerals.[2,6] Mineral frameworks in which calcite and ACC coexist in separate domains have also been reported.[7,8] Apart from skeletal functions, the ACC material appears to serve mostly as a depot for temporarily storing $CaCO_3$ units, which can later be released rather easily when needed due to the high solubility of ACC

[†] Institute of Physical and Theoretical Chemistry, University of Regensburg.
[‡] IACT (CSIC-UGR).
[§] University of Bayreuth.
[||] Institute of Microbiology and Archaeal Center, University of Regensburg.

(1) Addadi, L.; Weiner, S. *Angew. Chem., Int. Ed.* **1992**, *31*, 153.
(2) Addadi, L.; Raz, S.; Weiner, S. *Adv. Mater.* **2003**, *15*, 959.
(3) (a) Ogino, T.; Suzuki, T.; Sawada, K. *Geochim. Cosmochim. Acta* **1987**, *51*, 2757. (b) Brecevic, L.; Nielsen, A. E. *J. Cryst. Growth* **1989**, *89*, 504.
(4) Faatz, M.; Gröhn, F.; Wegner, G. *Adv. Mater.* **2004**, *16*, 996.
(5) Rieger, J.; Frechen, T.; Cox, G.; Heckmann, W.; Schmidt, C.; Thieme, J. *Faraday Discuss.* **2007**, *136*, 265.
(6) Taylor, M. G.; Simkiss, K.; Greaves, G. N.; Okazaki, M.; Mann, S. *Proc. R. Soc. London, Ser. B* **1993**, *252*, 75.
(7) Aizenberg, J.; Lambert, G.; Addadi, L.; Weiner, S. *J. Am. Chem. Soc.* **2002**, *124*, 32.
(8) Aizenberg, J.; Lambert, G.; Addadi, L.; Weiner, S. *Adv. Mater.* **1996**, *8*, 222.

relative to the crystalline phases.[2] In addition to permanently stable forms, it was shown that living systems also use transiently stabilized ACC as a solid precursor for calcification purposes, for instance during growth of sea urchin larval spicules[9] as well as mature spines[10] and teeth.[11] An apparent advantage in doing so is that amorphous matter, having no long-range crystalline order and preferred symmetry, can readily be molded in a predefined volume to adopt arbitrary shapes which are maintained upon recrystallization and hence imprinted on the forming crystal. This strategy was successfully applied to synthesize calcite single crystals with complex curved shapes[12] and patterned thin films.[13]

Stabilization of ACC *in vivo* seems to be regulated in general by specialized proteins, often in combination with magnesium ions,[7,14−16] or by extended organic membranes enclosing the amorphous phase.[17] Though not fully understood to date, protection mechanisms likely involve, as a key concept, kinetic inhibition of ACC transformation by hindering dissolution, delimiting exchange with the surrounding solution, or selectively impeding crystal growth. Also, the degree of hydration and the particular short-range order of the amorphous phase are important factors in this context.[18,19] Stable forms of biogenic ACC were found to incorporate appreciable amounts of water, typically 1 mol per mol of $CaCO_3$.[6,20] This structural water probably hampers reorganization into any of the anhydrous crystalline polymorphs.[2] In turn, when serving as a transient intermediate, ACC contains little to no water or transforms to a dehydrated state prior to crystallization.[9,10,15]

In-vitro precipitation experiments conducted in the presence of macromolecules extracted from ACC-comprising biominerals confirmed their stabilizing effect on the amorphous precursors.[8] Likewise, emulations of membrane-controlled biological $CaCO_3$ crystallization using self-assembled monolayers revealed that such organic matrices can direct and modify the formation of crystalline polymorphs from intermediate ACC.[21]

Apart from that, there have been various approaches to protect ACC precursors against crystallization by means of nonbiogenic additives. Rieger et al. demonstrated that soluble polycarboxylates adsorb on initially formed ACC particles and, at sufficiently high additive concentrations, cover their surface preventing dissolution and thus mineral scale formation.[5] Previous work had already shown that the lifetime of ACC in solution can be prolonged by addition of magnesium ions,[22] triphosphate,[23] or polyphosphonate species.[24] Remarkably stable micrometer-sized ACC particles, coexisting with calcite for up to two weeks, were furthermore observed by Donners et al. in the presence of certain dendrimer−surfactant mixtures.[25] With the aid of phytic acid as an inhibitor, Xu et al. prepared hollow ACC spheroids which developed due to the relative stability of hydrated ACC as compared to the anhydrous phase and persisted in solution for months without any discernible onset of crystallization.[26]

Additive-stabilized ACC intermediates have moreover proven to be versatile tools for $CaCO_3$ morphosynthesis and biomimetic mineralization.[27] For example, polymer-associated ACC particles can act as precursors for nanoscale crystalline building blocks used to construct higher-order architectures.[28] By precipitating initially an amorphous phase which is conserved by the polymers, transformation to crystalline polymorphs is decelerated and the design of complex ultrastructures through delicate crystal−polymer interactions becomes possible even at elevated supersaturation.[29]

Interestingly, most attempts reported so far to stabilize ACC and use it as a source for directed crystallization rely on the action of an *organic* additive or template, often following Nature's strategies in biomineralization. Herein, we show that the progress of calcium carbonate crystallization can be modified and controlled in a similar way also in simple *inorganic* precipitation systems. The presence of sodium silicate during precipitation of $CaCO_3$ from supersaturated solutions at elevated pH produced many of the effects discussed above for biological and biomimetic crystallization, that is, temporary or permanent storage of metastable ACC, delayed gradual transformation to crystalline polymorphs, and long-lasting coexistence of amorphous and crystalline phases, all based on the spontaneous deposition of siliceous skins around growing ACC particles.

2. Results

Effect of Silica on Growing ACC Particles. In a first set of experiments, particles precipitated from solutions containing 5 mM each of $CaCl_2$ and Na_2CO_3 and varying amounts of dissolved silica were investigated shortly after mixing by means of cryo-TEM (Figure 1 and S1 in the Supporting Information (SI)). In the absence of the additive, almost perfectly spherical particles with a mean diameter of 152 ± 36 nm are observed,

(9) (a) Beniash, E.; Aizenberg, J.; Addadi, L.; Weiner, S. *Proc. R. Soc. London, Ser. B* **1997**, *264*, 461. (b) Politi, Y.; Levi-Kalisman, Y.; Raz, S.; Wilt, F.; Addadi, L.; Weiner, S.; Sagi, I. *Adv. Funct. Mater.* **2006**, *16*, 1289. (c) Politi, Y.; Metzler, R. A.; Abrecht, M.; Gilbert, B.; Wilt, F. H.; Sagi, I.; Addadi, L.; Weiner, S.; Gilbert, P. U. P. A. *Proc. Natl. Acad. Sci. U.S.A.* **2008**, *105*, 17362.

(10) Politi, Y.; Arad, T.; Klein, E.; Weiner, S.; Addadi, L. *Science* **2004**, *306*, 1161.

(11) (a) Ma, Y.; Weiner, S.; Addadi, L. *Adv. Funct. Mater.* **2007**, *17*, 2693. (b) Killian, C. E.; Metzler, R. A.; Gong, Y. U. T.; Olson, I. C.; Aizenberg, J.; Politi, Y.; Wilt, F. H.; Scholl, A.; Young, A.; Doran, A.; Kunz, M.; Tamura, N.; Coppersmith, S. N.; Gilbert, P. U. P. A. *J. Am. Chem. Soc.* **2009**, *131*, 18404.

(12) (a) Loste, E.; Meldrum, F. C. *Chem. Commun.* **2001**, 901. (b) Li, C.; Qi, L. *Angew. Chem., Int. Ed.* **2008**, *47*, 2388.

(13) (a) Xu, G.; Yao, N.; Aksay, I. A.; Groves, J. T. *J. Am. Chem. Soc.* **1998**, *120*, 11977. (b) Aizenberg, J.; Muller, D. A.; Grazul, J. L.; Hamann, D. R. *Science* **2003**, *299*, 1205.

(14) Raz, S.; Weiner, S.; Addadi, L. *Adv. Mater.* **2000**, *12*, 38.

(15) Raz, S.; Hamilton, P. C.; Wilt, F. H.; Weiner, S.; Addadi, L. *Adv. Funct. Mater.* **2003**, *13*, 480.

(16) Tao, J.; Zhou, D.; Zhang, Z.; Xu, X.; Tang, R. *Proc. Natl. Acad. Sci. U.S.A.* **2009**, *106*, 22096.

(17) Beniash, E.; Addadi, L.; Weiner, S. *J. Struct. Biol.* **1999**, *125*, 50.

(18) Levi-Kalisman, Y.; Raz, S.; Weiner, S.; Addadi, L.; Sagi, I. *Adv. Funct. Mater.* **2002**, *12*, 43.

(19) Radha, A. V.; Forbes, T. Z.; Killian, C. E.; Gilbert, P. U. P. A.; Navrotsky, A. *Proc. Natl. Acad. Sci. U.S.A.* **2010**, *107*, 16438.

(20) Levi-Kalisman, Y.; Raz, S.; Weiner, S.; Addadi, L.; Sagi, I. *J. Chem. Soc., Dalton Trans.* **2000**, 3977.

(21) (a) Lee, J. R. I.; Han, T. Y.; Willey, T. M.; Wang, D.; Meulenberg, R. W.; Nilsson, J.; Dove, P. M.; Terminello, L. J.; Van Buuren, T.; De Yoreo, J. J. *J. Am. Chem. Soc.* **2007**, *129*, 10370. (b) Pichon, B. P.; Bomans, P. H. H.; Frederik, P. M.; Sommerdijk, N. A. J. M. *J. Am. Chem. Soc.* **2008**, *130*, 4034.

(22) Loste, E.; Wilson, R. M.; Seshadri, R.; Meldrum, F. C. *J. Cryst. Growth* **2003**, *254*, 206.

(23) Clarkson, J. R.; Price, T. J.; Adams, C. A. *J. Chem. Soc., Faraday Trans.* **1992**, *88*, 243.

(24) Sawada, K. *Pure Appl. Chem.* **1997**, *69*, 921.

(25) Donners, J. J. J. M.; Heywood, B. R.; Meijer, E. W.; Nolte, R. J. M.; Roman, C.; Schenning, A. P. H. J.; Sommerdijk, N. A. J. M. *Chem. Commun.* **2000**, 1937.

(26) Xu, A. W.; Yu, Q.; Dong, W. F.; Antonietti, M.; Cölfen, H. *Adv. Mater.* **2005**, *17*, 2217.

(27) (a) Meldrum, F. C.; Cölfen, H. *Chem. Rev.* **2008**, *108*, 4332. (b) Gower, L. B. *Chem. Rev.* **2008**, *108*, 4551.

(28) (a) Wang, T.; Cölfen, H.; Antonietti, M. *J. Am. Chem. Soc.* **2005**, *127*, 3246. (b) Cölfen, H.; Antonietti, M. *Angew. Chem., Int. Ed.* **2005**, *44*, 5576.

(29) Cölfen, H.; Qi, L. *Chem.−Eur. J.* **2001**, *7*, 106.

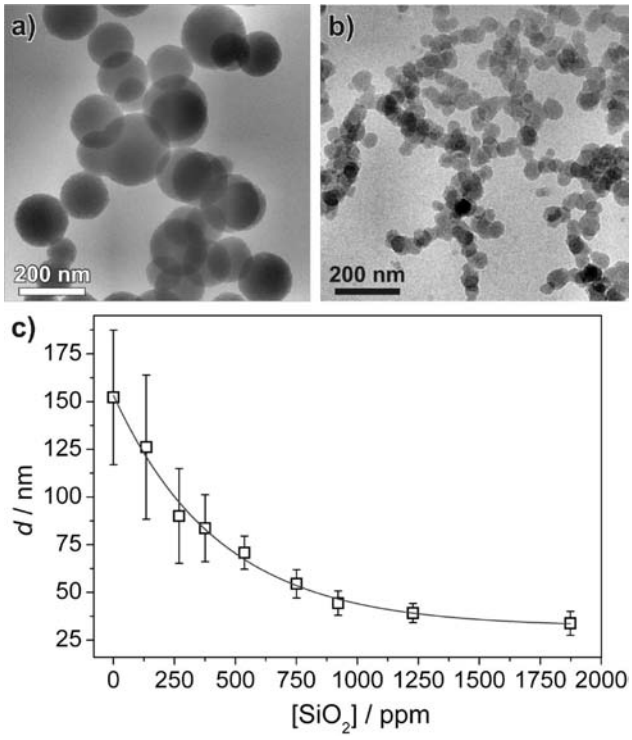

Figure 1. Effect of silica on the size, shape and aggregation behavior of ACC nanoparticles. (a, b) Cryo-TEM micrographs of samples vitrified after 1 min in the absence and presence (750 ppm) of silica, respectively. (c) Average particle diameter d and corresponding standard deviation as a function of the amount of added silica. Values were obtained by measuring at least 100 individual particles in the micrographs. The full line is a tentative first-order exponential decay fit to the experimental data, of the form $d = a_0 + a_1 \cdot \exp(-a_2 \cdot [SiO_2])$ (fit parameters: $a_0 = (31 \pm 7)$ nm, $a_1 = (123 \pm 26)$ nm, $a_2 = (443 \pm 125)$ ppm^{-1}, $R^2 = 0.989$).

in good agreement with earlier work conducted under similar conditions.[5] Addition of silica changes the situation dramatically. On the one hand, the size of primary grains decreases exponentially as more and more silica is added, from 126 ± 37 nm at 135 ppm over 55 ± 8 nm at 750 ppm down to eventually 34 ± 7 nm at 1870 ppm (Figure 1). Concomitantly, the size distribution of the particles becomes narrower, and the initially spherical contour is progressively distorted (see Figure S1 in the SI). On the other hand, particle agglomeration is distinctly more pronounced at higher silica concentrations. While spherules seem to maintain only loose contact and widely exist isolated from one another at low silica content, networks of densely aggregated particles extending over lengths of several hundreds of nanometers predominate in silica-rich environments. Corresponding powder samples obtained by filtration and subsequent freeze-drying were analyzed complementarily with the aid of scanning electron microscopy, yielding consistent results (Figure S2 in the SI).

The nature of the as-formed particles was characterized by electron diffraction, energy-dispersive X-ray analysis, and infrared spectroscopy. ED patterns in the frozen state suggest that all particles are amorphous, regardless of the amount of added silica (Figure S1 in the SI). Both EDX and IR data recorded using freeze-dried powders show that the silica content of the precipitates increases with the analytical solution concentration (see Figures S3 and S4 and Table S1 in the SI). Below 400 ppm, the fraction of silica in the particles is generally rather small (Si/Ca atomic ratio < 0.2), while it rises steeply above that threshold to reach values of up to Si/Ca ≈ 3 at the highest studied concentrations. Concurrently, IR bands at 1490, 1425, 1075, and 865 cm^{-1}, together with the lack of a defined peak around 710 cm^{-1}, identify amorphous calcium carbonate in all samples and prove the absence of crystalline polymorphs.[2,30] Further bands at 1643, 1036, 782, and 467 cm^{-1} can be assigned to amorphous silica and nonfree water.[31] We thus conclude that particles formed incipiently upon precipitation of $CaCO_3$ in silica-containing solutions are composites consisting of ACC and hydrated amorphous silica.

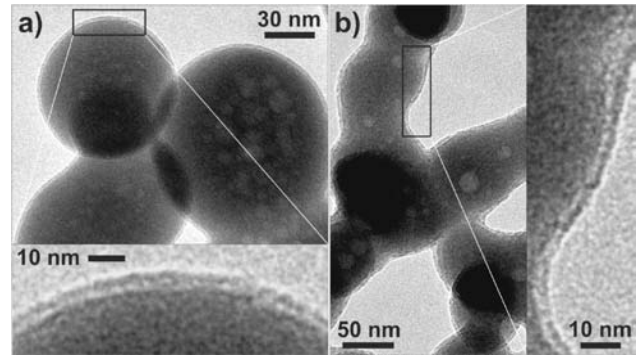

Figure 2. Electron micrographs evidencing the core−shell structure of the composite particles isolated 1 min after mixing at silica concentrations of (a) 270 and (b) 540 ppm. The average thickness of the shells was determined to be 2.1 ± 0.2 and 3.3 ± 0.8 nm in (a) and (b), respectively.

A closer look at samples prepared by blotting solutions on TEM grids reveals further structural details of the nanoparticles (Figure 2). Indeed, images resolve a thin layer of comparably low contrast sheathing a denser inner core. The thickness of these shells is in the range of 2 nm at 270 ppm SiO_2 and increases at higher additive concentrations, strongly suggesting that the skins are composed of silica and cover amorphous $CaCO_3$ particles. This notion is also supported by the observation that the core material tends to blister when irradiated, which is typical for calcium carbonate. Reference samples of pure silica were found to be stable under the same operating conditions. Apart from wrapping single ACC nanoparticles, the presumed silica skins seem to favor aggregation and interconnect grains by spanning a continuous envelope over multiple individuals.

Aggregation Behavior of Silica-Coated ACC Nanoparticles. Since the ACC particles are nucleated homogeneously throughout the system and remain suspended in the solutions for prolonged periods of time, aggregation effects can be monitored *in situ* by means of dynamic light scattering. Results show that the average diameter of scattering species increases linearly with time in both the absence and the presence of moderate amounts of the additive (0−270 ppm) and that this increase is faster as more silica is added (see Figure S5 in the SI). Apart from that, the size measured directly after mixing considerably exceeds that of discrete particles seen in TEM and SEM micrographs. Precipitation runs quenched at later stages prove that individual particles do not grow further with time, also in silica-free systems. In light of these findings, the formation of ACC in the present experiments seems to be completed, more or less quantitatively, soon after mixing (≤ 1 min). Consequently, the DLS data directly reflect aggregation processes and thus demonstrate that silica promotes the agglomeration of primary grains. Ample conjunction of particles is probably driven by

(30) Andersen, F. A.; Brecevic, L. *Acta Chem. Scand.* **1991**, *45*, 1018.
(31) Martínez, J. R.; Ruiz, F.; Vorobiev, Y. V.; Pérez-Robles, F.; González-Hernández, J. *J. Chem. Phys.* **1998**, *109*, 7511.

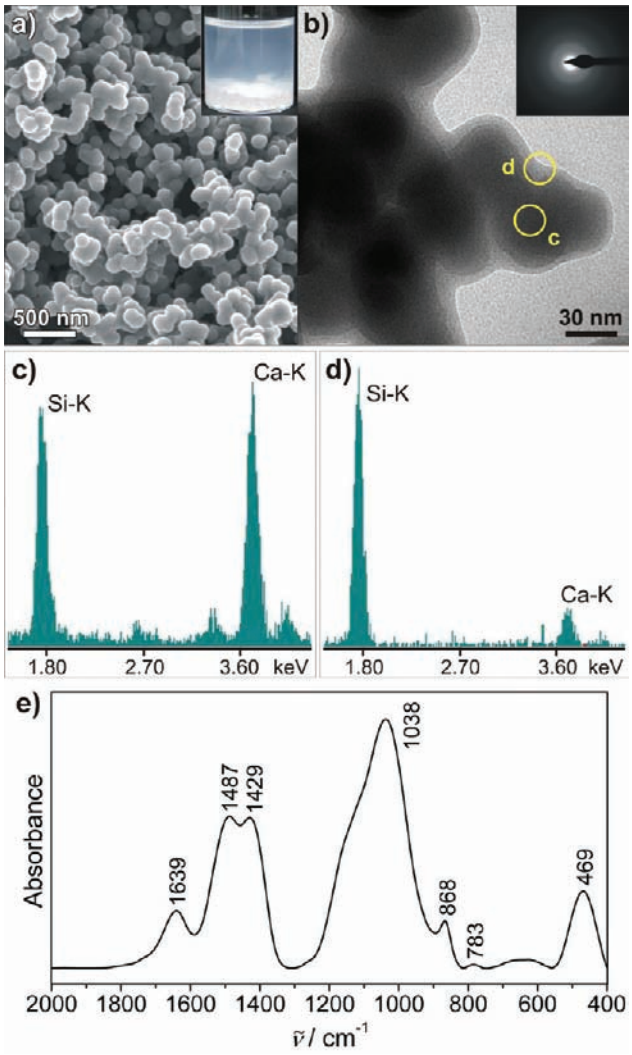

Figure 3. Flocculation of ACC−silica composites in mixtures at 750 ppm SiO_2 after 90 min. (a) FESEM image of the isolated solid showing networks of conflated nanoparticles, and a corresponding photograph illustrating sedimentation in the vials (inset). (b) TEM micrograph disclosing the structure of the floccules, and an electron diffraction pattern proving that the material is completely amorphous. Microanalyses of the dark inner region (c) and the lighter border area (d) strongly suggest that the core of the particles is rich in $CaCO_3$ while the outer layer consists of silica. The mean thickness of the shells is 9.4 ± 3.3 nm. (e) Infrared spectrum of the precipitate with bands characteristic of ACC and silica.

condensation reactions of free silanol groups between coating siliceous layers which cause the silica to act like a glue sticking individuals together.

At higher silica concentrations (375−750 ppm), particle agglomeration becomes more and more enhanced and fairly large assemblies are formed within a few minutes, which coalesce macroscopically leading to sedimentation of a fluffy precipitate. To shed light on their composition, floccules at 750 ppm SiO_2 were isolated after 90 min and analyzed in detail (Figure 3). Samples were found to be fully amorphous, showing IR characteristics typical for ACC and silica. Notably, there were also no crystals discernible on the walls or the surface of the solution. Hence, $CaCO_3$ exists still entirely as ACC. The flocs are composed of densely aggregated distorted nanoparticles which exhibit evident core−shell morphology. In this concentration regime, the outer layer is very distinct and reaches a thickness of more than 10 nm, permitting EDX microanalysis of the shell region. Comparison of the data to those collected

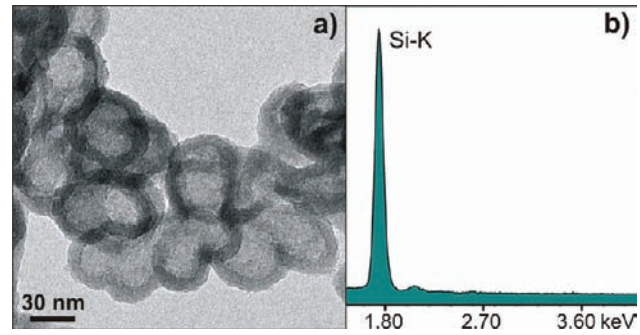

Figure 4. Selective carbonate dissolution. (a) Hollow silica particle networks obtained by leaching samples prepared at 750 ppm SiO_2 in dilute acid. The average wall thickness is 9.0 ± 1.1 nm. (b) EDX profile demonstrating the absence of Ca.

from the core indicates that the Ca signal drops when approaching the border of the particles while the Si count remains high. The Si/Ca ratio detected for the floccules (1.46) is significantly higher than in early particles isolated after 5 min at the same silica concentration (1.17), indicating that silica precipitation proceeds over extended frames of time.

Leaching Experiments. A final proof for the outer skins being silica can be given by treating the precipitates with acid. For this purpose, freeze-dried powders from a sample at 750 ppm silica were immersed in dilute HCl for several days, after which the gross part of the material had vanished. The remaining limpid floccules were studied with TEM, revealing hollow particles and networks thereof (Figure 4).

Acidifying the samples obviously leads to selective dissolution of the labile carbonate component from the particles, whereas the siliceous fraction is sparsely soluble and persists at low pH. This implies that the silica layers coating the ACC precursors must be porous and allow for exchange with the surrounding medium. At the chosen silica concentration, a certain percentage of unaffected grains were sighted next to hollow ones, suggesting different degrees of skin porosity. Remarkably, the silica shells do not collapse during dissolution and the original morphology of the ACC particles is reflected in the shape of the silica remnants. The thickness of the walls decreases a little upon leaching, due to either contraction caused by protonation or slight etching. We note that Chen et al. prepared hollow silica particles with comparable sizes and morphologies following a similar procedure.[32] However, these authors used prefabricated calcite nanoparticles as templates onto which silica was deposited in a second step by controlled polymerization. This is in sharp contrast to the present experiments where direct coprecipitation of $CaCO_3$ and silica produced the core−shell particles at once.

Effect of Silica on the Transformation of ACC to Stable Calcite. Based on the above findings, the progress of ACC transformation to crystalline polymorphs was followed with time by repeatedly quenching and characterizing samples until its completion, when only crystals and a clear solution remained. Without added silica, ACC was found to be the only phase present still after 10 min, while first crystalline products were detected after 30 min (Figure S6 in the SI). With proceeding crystal growth, the ACC fraction decreases, although significant amounts of amorphous particles could still be discerned even after 60 min. ACC hence persisted substantially longer in our

(32) Chen, J.-F.; Wang, J.-X.; Liu, R.-J.; Shao, L.; Wen, L.-X. *Inorg. Chem. Commun.* **2004**, *7*, 447.

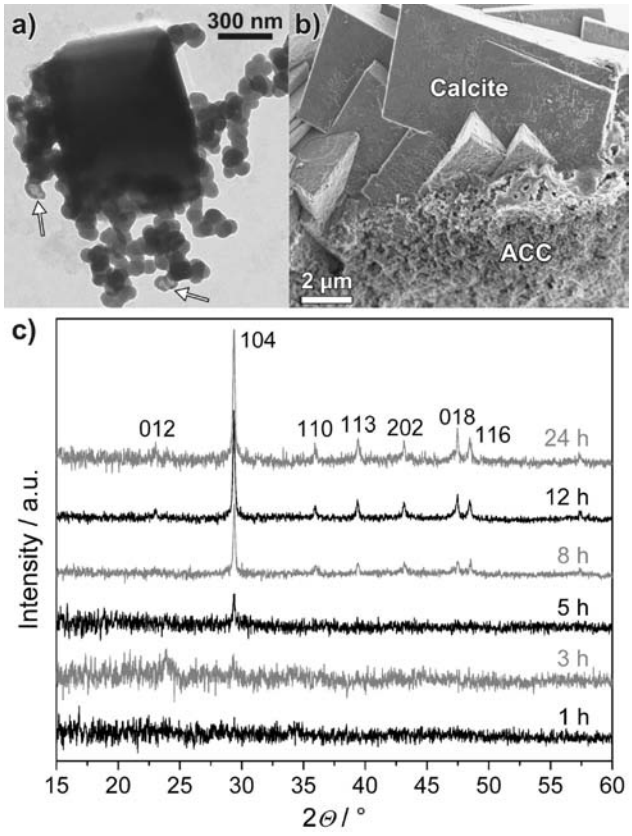

Figure 5. Recrystallization of calcite from temporarily silica-stabilized ACC particle networks. (a) TEM image of a rhombohedral calcite crystallite nucleated on top of the precursor particles. Arrows indicate nanoparticles that appear to be hollow (375 ppm SiO_2, 90 min). (b) FESEM micrograph showing the boundary between amorphous particle floccules and calcite crystals which grow nourished by the inner ACC fraction of the core−shell particles (270 ppm SiO_2, 60 min). (c) Powder diffraction patterns of precipitates (both amorphous floccules and, if present, crystals) isolated from mixtures at 750 ppm SiO_2 after different times. The emergence of a weak calcite (104) peak after 5 h indicates the onset of crystallization. With time, further calcite reflections appear and the intensity of the signal increases.

experiments than in earlier studies at the same supersaturation.[5] Most probably, discrepancies arise as a consequence of different mixing conditions. Eventually, after 90 min, only characteristic calcite rhombohedra and very rarely also vaterite spheres were observed. Crystals thereby formed essentially on the walls of the vials or the surface of the solutions, thus strongly suggesting heterogeneous nucleation.

Addition of silica essentially results in a stabilization of amorphous precursor particles and a marked retardation of crystallization. At 270 ppm SiO_2, ACC particles were observed still after 90 min (Figure S7 in the SI), while samples with 375 ppm were entirely amorphous at the same time (confirmed by XRD data). Powder diffraction patterns as well as SEM and TEM images disclose that at 540 ppm no crystalline polymorphs are formed before 3 h. After the respective delay, calcite microcrystallites are nucleated within the precipitated floccules and grow adjacent to the particle networks (Figure 5a,b). A closer look at precursor particles associated to a developing crystal reveals that some of them are hollow. Apparently, the inner ACC core was dissolved in order to supply $CaCO_3$ for crystal growth, which is supported by the finding that the Ca/Si atomic ratio of the amorphous fraction decreases successively with time (Figure S7 in the SI). This indicates that in the presence of silica the transformation of ACC to stable calcite occurs via a dissolution−reprecipitation pathway, as reported previously for the crystallization of $CaCO_3$ in the absence of additives.[33] Sheathing by silica prevents possible solid-state conversions as the ACC particles lack mutual contact and can therefore not merge. The fact that crystals grow directly on the amorphous floccules likely derives from the elevated supersaturation in the vicinity of particle aggregates which gradually release $CaCO_3$ units and, in addition, provide a surface facilitating nucleation. After equilibration, calcite crystals were the only solid product remaining in the vials while all nanoparticles, including the hollow ones, had vanished. This implies that, at silica concentrations of up to 540 ppm, conversion of ACC to calcite is quantitative and that the silica skin redissolves in the mother liquor once the inner ACC core had been detached. Thus, precipitation of silica seems to be favored only under the conditions prevailing locally around the ACC particles, but not under those existing in the bulk solution. Redissolution of silica is likely to be supported by ongoing disintegration of the ACC core, which raises the pH and thus the solubility of silica in the vicinity of the particles.

When the silica content is increased further, a growing percentage of the precursor particles become sheathed by skins dense enough to permanently prevent dissolution and recrystallization. For example, at 750 ppm SiO_2, powder diffraction data show that calcite formation commences after a delay of roughly 4−5 h and proceeds for up to about 1 day (Figure 5c). Subsequently, no further change in the fraction of crystalline material (assessed by integration of the calcite (104) reflex) could be discerned even when the system was left to evolve for periods as long as 1 year (Figure S8 in the SI). Optical micrographs and FESEM images yet clearly illustrate that a major part of the samples is still constituted by amorphous floccules after such extended frames of time. Separate analyses of the floccules by EDX spectroscopy reveal that, upon apparent completion of crystallization, around 58% of the total molar amount of Ca present is still enclosed in the nanoparticle networks (Figure S9 in the SI). Infrared spectra of powder samples isolated after 1 year verify the presence of both ACC and calcite (Figure S10 in the SI). Furthermore, the calculated intensity ratio of the υ_2 (~870 cm^{-1}) and the υ_4 (~700 cm^{-1}) mode was used to estimate, according to previous work,[15] the overall ACC fraction in the sample to be about 50%. Hence, after conversion of insufficiently protected ACC within the first 24 h after mixing, compositionally stable systems are obtained in which amorphous calcium carbonate and calcite coexist without notable changes over time scales of years. To our knowledge, stabilization of ACC in contact with its mother solution for such extended periods of time has not been reported to date.

Finally, at values well above 1000 ppm, all ACC material is effectively cemented in a siliceous matrix such that transformation to calcite is completely inhibited. Characterization of samples at 1870 ppm SiO_2 that were left to stand for more than 1 year confirms that protection of ACC precursors is an enduring effect under these conditions (Figure 6). SEM and TEM images evidence that the isolated precipitates still consist entirely of rounded nanoparticles with no specific crystalline shapes distinguishable. X-ray diffraction patterns identify the material as being fully amorphous, while IR spectra indicate the presence

(33) (a) Rieger, J.; Thieme, J.; Schmidt, C. *Langmuir* **2000**, *16*, 8300. (b) Pontoni, D.; Bolze, J.; Dingenouts, N.; Narayanan, T.; Ballauff, M. *J. Phys. Chem. B* **2003**, *107*, 5123. (c) Wolf, S. E.; Leiterer, S.; Kappl, M.; Emmerling, F.; Tremel, W. *J. Am. Chem. Soc.* **2008**, *130*, 12342.

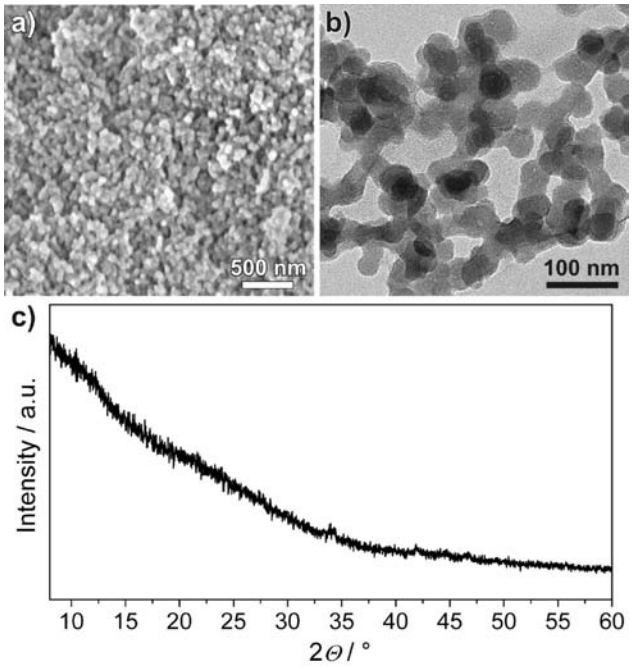

Figure 6. Long-term stabilization of amorphous calcium carbonate at 1870 ppm SiO_2. (a) FESEM image of particles isolated from a sample after 1 year. (b) TEM micrograph of a dried sample displaying multiple spherical nanoparticles embedded in a translucent matrix. (c) XRD pattern of the particles verifying the absence of any crystalline matter.

of calcium carbonate, most probably as ACC, next to an appreciable amount of amorphous silica (Figure S10 in the SI). With the corresponding EDX data (Table S1 in the SI) and the assumption that the stoichiometry of the components is properly described by $CaCO_3$ and SiO_2, the average mass fraction of ACC in the particles at 1870 ppm can be estimated to be about 36.5%.

The diameter of primary ACC grains ranges typically between about 30 and 40 nm and does not change noticeably with time (Figure 6b). Recently, Pouget et al. observed that particles with similar sizes were the first ACC species formed upon nucleation in the course of $CaCO_3$ crystallization.[34] This may hint at ACC becoming enveloped by the silica at 1870 ppm immediately, or soon, after nucleation such that the smallest possible particles are stabilized. The crystallization process is thus frozen at an extremely early stage.

3. Discussion

Our findings can be rationalized in a mechanism as depicted in Scheme 1. Upon mixing $CaCl_2$ and Na_2CO_3, amorphous calcium carbonate is instantly nucleated throughout the solution in the form of spherical nanoparticles (Stage 1). At the given high pH of the mixtures, carbonate ions are expected to coexist to a considerable extent with bicarbonate (see Section S3 in the SI). For instance, the fraction of HCO_3^- ions in equilibrium 2 min after mixing amounts to about 30−40% depending on the silica concentration (Table S2). Growth of ACC induces dissociation of bicarbonate and the release of protons according to

$$HCO_3^- \rightleftharpoons CO_3^{2-} + H^+ \xrightarrow{Ca^{2+}} CaCO_3\downarrow$$

This should result in a decrease of pH around the surface of growing particles relative to the outer alkaline bulk (Stage 2).[35] Within the presumed local pH gradient, the solubility of silica will be markedly reduced (see Section S3 in the SI) as protonation of silicate species becomes enhanced and silanol groups liable to condensation reactions are formed:

$$\text{-Si-O}^- + H^+ \rightleftharpoons \text{-Si-OH} + \text{HO-Si-} \xrightarrow{-H_2O} \text{-Si-O-Si-} \longrightarrow \text{“SiO}_2\text{”}\downarrow$$

The nascent protons thus create $Si(OH)_4$ species that condense in rapid succession to higher oligomers, polymeric fragments, and small colloidal particles,[36,37] which finally precipitate on the ACC grains (Stage 3). Deposition of silica nanoparticles on the carbonate surface will initially generate an inhomogeneous and porous layer with an uneven topology, causing an apparent distortion of the original spherical shape especially at higher silica concentrations (cf. Figures 1 and S1). According to Iler, the solubility equilibrium of a silica surface depends on the local curvature, with concave regions being essentially less soluble than convex ones.[36] Therefore, after initial pH-induced coagulation further dissolved silicate will be incorporated to the layers in order to fill concave crevices between the colloids, which progressively flattens the surface. This explains the detected increase in the Si/Ca ratio of the particles with time and suggests that the shells densify rather than continually grow in thickness. Eventually, these precipitation processes produce a smooth and homogeneous skin of amorphous silica all over the ACC particles (Stage 4), the final thickness and density of which is determined by the overall degree of polymerization and hence, among others, the concentration of silica. Coating of ACC by consolidated siliceous shells arrests growth and consequently defines the size of the particles, which become smaller when the amount of added silica is increased. The presence of external skins constrains dissolution and avoids potential Ostwald ripening. Therefore, energetically favored transformation to crystalline polymorphs is inhibited and usually transient ACC species are stabilized. Moreover, condensation reactions between the superficial silica layers promote aggregation of the core−shell particles yielding extended networks of tightly conjoint and necked individuals (Stage 5).

Depending on the specific silica concentration we found two limiting cases. Below 1000 ppm, calcite crystallizes after a certain delay at the expense of the ACC precursors since the skins around the particles are not sufficiently dense to prevent dissolution and subsequent nucleation of the stable phase in the long term (Stage 6a). Above 1000 ppm, extensive silica polymerization leads to the formation of “leak-proof” coatings which allow for a permanent conservation of ACC on time scales of years (Stage 6b). At concentrations ranging from 750 to about 1000 ppm, effective stabilization is sustained only for a distinct fraction of the particles such that ACC and calcite coexist side by side in equilibrium. This implies that the degree of silica condensation may vary between individual particles under these conditions, thus leading to shells of potentially different porosity and/or thickness. In fact, the porosity of precipitated nanoscale silica coatings and their permeability for small molecules and ions have been demonstrated in earlier work

(34) Pouget, E. M.; Bomans, P. H. H.; Goos, J. A. C. M.; Frederik, P. M.; De With, G.; Sommerdijk, N. A. J. M. *Science* **2009**, *323*, 1455.
(35) García-Ruiz, J. M.; Melero-García, E.; Hyde, S. T. *Science* **2009**, *323*, 362.
(36) Iler, R. K. *The Chemistry of Silica*; Wiley: New York, 1979.
(37) (a) Conrad, C. F.; Icopini, G. A.; Yasuhara, H.; Bandstra, J. Z.; Brantley, S. L.; Heaney, P. J. *Geochim. Cosmochim. Acta* **2007**, *71*, 531. (b) Navrotsky, A. *Proc. Natl. Acad. Sci. U.S.A.* **2004**, *101*, 12096.

Scheme 1. Mechanism for Silica-Mediated Stabilization of Amorphous Calcium Carbonate and Control over Calcite Crystallization[a]

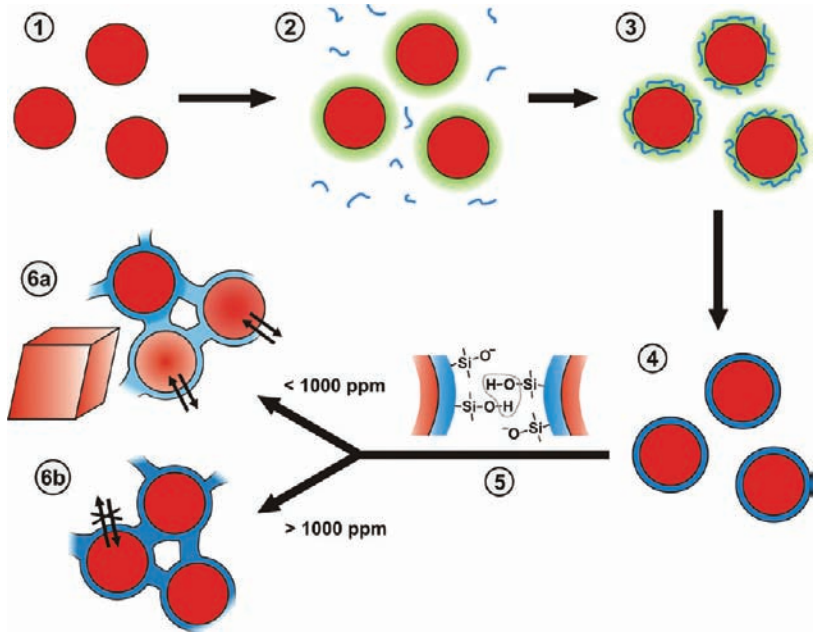

[a] In alkaline solutions, growing ACC nanoparticles (red circles) generate pH gradients (green) over their surfaces due to dissociation of bicarbonate ions. Silicate species (blue) respond to these local changes by polymerization reactions which prompt in-situ precipitation of expanded silica skins around the particles (Stages 1−4). Condensation of superficial silanol groups favors particle aggregation and provokes flocculation of an amorphous ACC−silica composite material (Stage 5). Ultimately, calcite crystals are formed by transformation of ACC via dissolution-renucleation processes at silica concentrations of up to 1000 ppm (Stage 6a). Above that threshold, ACC precursors become cemented in siliceous matrices to such an extent that exchange with the solution is no longer possible and crystallization is completely and permanently prevented (Stage 6b). Note that structures are not drawn to relative scale.

dealing with metal nanoparticles.[38] In line with the present results, it was reported that both the thickness and the density of the silica layers determine the rate of exchange between the core material and the surrounding solution and whether the particles are pervious to reagents or not.

Previous analyses on the composition of synthetically produced ACC have shown that the phase generated on precipitation usually contains water in variable amounts.[3a,19,39] Therefore, we suspect that the ACC formed in our experiments is also hydrated to a certain, yet unknown degree. In this regard, the role of the silica shells in stabilizing the amorphous particles may not be confined to acting as a barrier which delimits the release of ions into the solution and hence restrains dissolution of ACC. In addition, they might prohibit the expulsion of water molecules from the core and, thereby, prevent possible transformations of hydrated ACC to anhydrous crystalline polymorphs inside the compartments.[2]

The experiments described in this work illustrate that the addition of silica is a powerful means to concertedly modify the progress of $CaCO_3$ crystallization. Simply by adjusting the silica concentration, ACC can be either stabilized temporarily or permanently or allowed to coexist with tunable fractions of calcite. Living organisms retain similar, yet surely by far more sophisticated control over the stability of ACC in- and outside their tissues.[2,9−11,14−18,20] Nevertheless, it is surprising to which extent the delicate processes occurring in biological and bioinspired synthetic environments can be emulated in purely *inorganic* systems. This analogy is additionally fuelled by the ability of silica to produce exceptional crystal architectures of alkaline-earth carbonates reminiscent of biogenic forms, as already recognized in previous studies.[40] In the present work, calcite crystals isolated at elevated silica concentrations exhibited as well morphologies and structures of remarkable complexity, a detailed description of which will be provided in a forthcoming publication. We note, however, that the key to structured crystallization under the given conditions lies in the temporary storage of $CaCO_3$ as silica-sheathed ACC and the concurrent relief of actual supersaturation. This is another strategy also applied in biomineralization.[2]

Our results may have implications also for other areas of research. For instance, the finding that at high silica concentrations crystallization of calcium carbonate is completely avoided has obvious potential for the field of scale inhibition, especially in light of recent considerations to operate desalination facilities at elevated feedwater pH.[41] Further, geological scenarios leading to the frequent common occurrence of carbonate minerals and silica in sediments,[42] selective incrustation phenomena,[43] and the formation of replacement cherts[44] might have involved interactions related to those identified herein. Finally, our experiments demonstrate that directly precipitating calcium carbonate in the presence of sodium silicate is a straightforward one-step route for the production of well-defined silica-coated

(38) Giersig, M.; Ung, T.; Liz-Marzán, L. M.; Mulvaney, P. *Adv. Mater.* **1997**, *9*, 570.
(39) (a) Koga, N.; Nakagoe, Y.; Tanaka, H. *Thermochim. Acta* **1998**, *318*, 239. (b) Koga, N.; Yamane, Y. *J. Therm. Anal. Calorim.* **2008**, *94*, 379.
(40) (a) García-Ruiz, J. M.; Hyde, S. T.; Carnerup, A. M.; Christy, A. G.; Van Kranendonk, M. J.; Welham, N. J. *Science* **2003**, *302*, 1194. (b) Imai, H.; Terada, T.; Yamabi, S. *Chem. Commun.* **2003**, 484. (c) Voinescu, A. E.; Kellermeier, M.; Bartel, B.; Carnerup, A. M.; Larsson, A. K.; Touraud, D.; Kunz, W.; Kienle, L.; Pfitzner, A.; Hyde, S. T. *Cryst. Growth Des.* **2008**, *8*, 1515.
(41) Andrews, B.; Davé, B.; López-Serrano, P.; Tsai, S. P.; Frank, R.; Wilf, M.; Koutsakos, E. *Desalination* **2008**, *220*, 295.
(42) Kitano, Y.; Okumura, M.; Idogaki, M. *Geochem. J.* **1979**, *13*, 253.
(43) Frondel, C. *Am. Mineral.* **1937**, *22*, 1104.
(44) Klein, R. T.; Walter, L. M. *Chem. Geol.* **1995**, *125*, 29.

$CaCO_3$ nanoparticles, which have attracted attention due to their beneficial properties in view of distinct applications.[45]

4. Conclusion

In summary, we have shown that the coupling between the speciations of carbonate and silicate in alkaline solutions can be exploited to coat ACC nanoparticles *in situ* during precipitation with skins of amorphous silica. This results in suppression of chemical exchange with the surrounding medium and substantial inhibition of ACC transformation to calcite. The porosity of the silica layer around the precursor particles and hence the degree of stabilization were found to be a function of the silica concentration, ranging from slightly prolonged lifetimes of ACC to permanent conservation over years. Overall, the dynamic interplay between components maintains discrete control over ACC stability and the rate of calcite crystallization and, thus, imitates in the absence of organic matter strategies recently identified to be used by various living organisms for concerted $CaCO_3$ mineralization. The concepts devised in this study might, in all likelihood, be readily transferable to compounds other than calcium carbonate, which are likewise capable of generating local pH gradients during growth in alkaline media.

5. Experimental Section

Calcium carbonate precipitation was initiated by directly mixing 10 mM solutions of calcium chloride and sodium carbonate, the latter containing different amounts of sodium silicate (0−4000 ppm as SiO_2). The starting pH was essentially determined by the concentration of the additive and varied within a range of 10.4−10.8 (see Section S3 in the SI). Afterward, samples were left to evolve under quiescent conditions at ambient temperature. Parameters like the volume of the reagents or the speed, and particularly the order of mixing, were found to affect the behavior of the samples. Therefore, special care was taken to maintain the mixing procedure throughout this work, and experiments were repeated several times to ensure reproducibility.

Upon combining reagents, all samples turned turbid instantaneously as amorphous nanoparticles were nucleated homogeneously in the solutions. Turbidity persisted in the systems for different periods of time depending on the silica concentration, indicating that nanoparticles stayed suspended in the mixtures. As transformation of ACC proceeded, the solutions gradually became clearer until finally only crystals grown on the bottom and the walls of the vials remained. The presence of silica induced the formation of an optically isotropic fluffy precipitate, which settled to the bottom leaving a still turbid solution on top. The time after which flocculation occurred, usually ranging from about 60 to 90 min, and the amount of the precipitated material varied with the additive concentration.

Suspended particles and flocculated precipitate were isolated together at distinct times after mixing by filtration and immediate freeze-drying, in order to prevent uncontrolled transformation of ACC material. Freeze-dried samples were examined with a variety of techniques including field-emission scanning electron microscopy (FE-SEM), X-ray diffraction (XRD), and energy-dispersive X-ray (EDX) as well as infrared (IR) spectroscopy. Alternatively, the as-formed particles were characterized using transmission electron microscopy (TEM) in combination with electron diffraction (ED) and micro-EDX analysis. To that end, aliquots of the particle suspensions were blotted on TEM grids to give a thin layer of liquid, which was either quickly frozen and studied in a vitrified state (cryo-TEM) or left to dry in air and inspected at room temperature. Further details on experimental procedures and methods are given in the Supporting Information (Section S1).

Acknowledgment. The authors thank Martina Heider, Benjamin Gossler, and Werner Reichstein (University of Bayreuth) for access to the scanning electron microscope and help with the analyses. We are further grateful to Martina Andratschke for carrying out powder diffraction measurements as well as Hannes Krauss (both University of Regensburg) for support during the IR analyses. M.K. appreciates the granting of a scholarship by the Fonds der Chemischen Industrie. Financial support by the Deutsche Forschungsgemeinschaft (SFB 481) (M.D.) and the program Juan de la Cierva of the Spanish Science Ministry (MICINN) (E.M.G.) is gratefully acknowledged.

Supporting Information Available: Detailed description of experimental procedures and the techniques used (Section S1), supplementary Figures S1−S10 and Table S1 (Section S2), pH data and graphs illustrating changes in speciations and solubility with pH (Section S3, including Figures S11−S13 and Table S2). This material is available free of charge via the Internet at http://pubs.acs.org.

JA106959P

(45) Bala, H.; Zhang, Y.; Ynag, H.; Wang, C.; Li, M.; Lv, X.; Wang, Z. *Colloids Surf., A* **2007**, *294*, 8.